Journal of Alloys and Compounds 636 (2015) 211–215

Contents lists available at ScienceDirect

Journal of Alloys and Compounds

journal homepage: www.elsevier.com/locate/jalcom

Synthesis and characterization of Cr^{4+}-doped Ca_2GeO_4 tunable crystal

Chun Li [a], Jialin Xu [a], Wang Liu [a], Dongyang Zheng [a], Shanli Zhang [a], Ying Zhang [b], Hai Lin [a], Lina Liu [a], Jinghe Liu [a], Fanming Zeng [a,*]

[a] Engineering Research Center of Optoeletronic Functional Materials, Ministry of Education, School of Materials Science and Engineering, Changchun University of Science and Technology, Changchun 130022, China
[b] Changchun Institute of Optics, Fine Mechanics and Physics, Chinese Academy of Sciences, Changchun 130033, China

ARTICLE INFO

Article history:
Received 4 November 2014
Received in revised form 13 February 2015
Accepted 16 February 2015
Available online 23 February 2015

Keywords:
Cr^{4+}:Ca_2GeO_4 crystal
Structure characterization
Spectral analysis

ABSTRACT

The growth, structure and spectral properties of a Cr^{4+}:Ca_2GeO_4 single crystal have been reported in this paper. XPS analysis demonstrated that the chromium in the single crystal is tetravalent; this is further confirmed by fluorescence spectroscopy. The near-infrared, visible absorption and near-infrared luminescence spectrum of the Cr^{4+}:Ca_2GeO_4 crystal are presented in this paper. In the absorption spectra, the transitions from the $^3A_2$ ground state to the three orbital components of the $^3T_1$ and $^3T_2$ excited state are observed. The range of the fluorescence spectroscopy band of the Cr^{4+}:Ca_2GeO_4 crystal at room temperature is from 1000 nm to 1600 nm. The single band with a maximum peak at 1317 nm at room temperature is attributed to the $^3T_2 \rightarrow {}^3A_2$ transition of the Cr^{4+} ions. The FWHM of the fluorescence spectrum is 201.19 nm, and the fluorescence lifetime and emission cross section are up to 12 μs and 4.61×10^{-19} cm^2, respectively.

1. Introduction

Diode pumped passively Q-switched laser produces high peak power and high repetition rate laser light in the nanosecond and sub-nanosecond range, which is characterized by compact structure, economy, and solidification [1,2]. This laser can be widely used in radar, ranging, remote sensing, nonlinear optical processing, and material processing [3–6]. Cr^{4+} ions in a crystal show great potential for use in a tunable solid-state laser in the spectral range of 1.1–2 μm at room temperature [7]. Cr^{4+} ion laser crystal mainly includes Cr^{4+}:YAG [8,9]. The main absorption bands of the crystals include 0.48 μm, 0.65 μm, and 1 μm. The absorption transition that is excited from ground state $^3A_2$ to state $^3T_1$ results in 0.65 μm absorption band, whereas 1 μm infrared absorption band is the result of absorption transition that is excited from ground state $^3A_2$ to state $^3T_2$. Cr^{4+}:YAG crystal growth, spectroscopic properties, and laser properties were studied [10,11]. Moreover, the research indicated that not only 1.06 μm Nd:YAG is the ideal pump source of Cr^{4+}:YAG, but also InGaAs high-power diode is the preferred pump source of Cr^{4+}:YAG lasers, which are toward all-solid state and miniaturization. Cr^{4+}:YAG crystal have large amounts of Cr^{3+} ions as impurities, leading to low Cr^{4+} concentrations and reducing the figure of merit in the crystal [12,13]. Cr^{4+}:YAG crystal requires a charge-compensating codopant during crystal growth process. In addition, the nonradiative relaxation of the laser level is significant in Cr^{4+}:YAG crystals. Moreover, the fluorescence-quenching effect of Cr^{4+}:Ca_2GeO_4 is significantly less than that of Cr^{4+}:Ca_2GeO_4 at room temperature. Therefore, Cr^{4+}:Ca_2GeO_4 crystal is a promising near-infrared laser material. Researchers state that these crystals are ideal optical communication tunable laser crystals. Several wide practical applications, such as in medicine, telecommunication fiber sensing, and semiconductor diodes, have been recently demonstrated for Cr^{4+}:Ca_2GeO_4 crystal [14–18]. In this paper, we present the flux growth and properties of the Cr^{4+}:Ca_2GeO_4 crystal.

2. Experimental details

In this experiment, Cr_2O_3(5N), GeO_2(5N), $CaCO_3$ (analytical grade) and $CaCl_2$ (analytical grade) were used as reagents. The Cr^{4+}:Ca_2GeO_4 crystal was grown by the flux growth method from the flux of $CaCl_2$ with a Ca_2GeO_4 concentration of 65 wt.% and a Cr_2O_3 concentration of 0.5 wt.%. The crystallization parameters were as follows: growth direction is [100]; the platinum wire seeding temperature range was 700–1000 °C; the pulling rate was 0.1–0.2 mm/h; the seed rotation speed was 20–60 rpm; the growth atmosphere was oxygen. Finally, the fully transparent, dark-green Cr4+:Ca_2GeO_4 crystals with more than ∅15 mm × 60 mm were been grown under the growth conditions. In this experiment, the GeO_2 content was in excess by 5–8% to account for the volatility of GeO_2 at the high temperatures used. The crystal image is shown in Fig. 1.

* Corresponding author at: Engineering Research Center of Optoeletronic Functional Materials, Ministry of Education, Changchun University of Science and Technology, Changchun, Jilin 130022, China.
E-mail address: zengfm@126.com (F. Zeng).

http://dx.doi.org/10.1016/j.jallcom.2015.02.121
0925-8388/

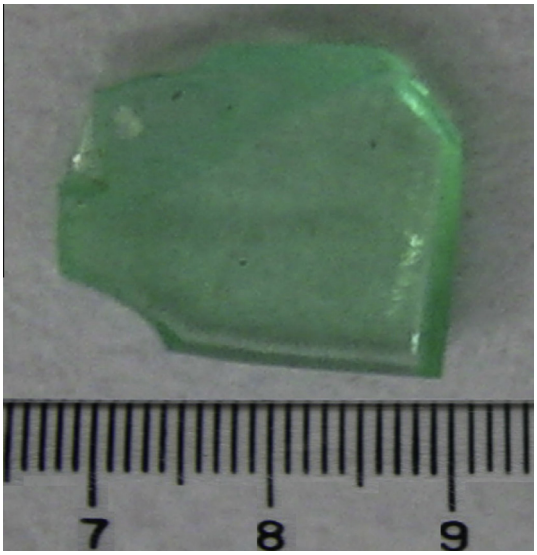

Fig. 1. Image of Cr^{4+}:Ca_2GeO_4 crystal.

3. Results and discussion

3.1. The formation mechanism of the Cr^{4+} ion

In the case of a Cr^{4+}:Ca_2GeO_4 crystal grown by the flux method, the Cr^{4+} ion was obtained by oxidizing of Cr^{3+} from Cr_2O_3 in the oxygen atmosphere with the Ca element added to the melt as a charge compensator. The roles of Ca and O_2 are explained using the following chemical reaction [19]:

$$4Cr^{3+} + 2\left(V_O^{2+} + 2Ca^{2+}\right) + O_2 \rightarrow 4Cr^{4+} + 4Ca^{2+}$$

where V_O^{2+} indicates the oxygen vacancy in the crystal.

The powder X-ray diffraction results for the 0.5 wt.% Cr^{4+}:Ca_2GeO_4 single crystal are shown in Fig. 2. A single phase of the Ca_2GeO_4 with no additional peaks indicates that Cr^{4+} has been successfully incorporated in the crystal by the flux method. The result is in accordance with the standard JCPDS card (No. 26-0304). According to the JCPDS26-0304 card, the crystal structure can be indexed as an olivine-type structure. According to the diffraction formula:

$$2d\sin(\theta) = n\lambda \quad (1)$$

When $n = 1$, this formula can be written as follows: $d = \lambda/2\sin(\theta)$.

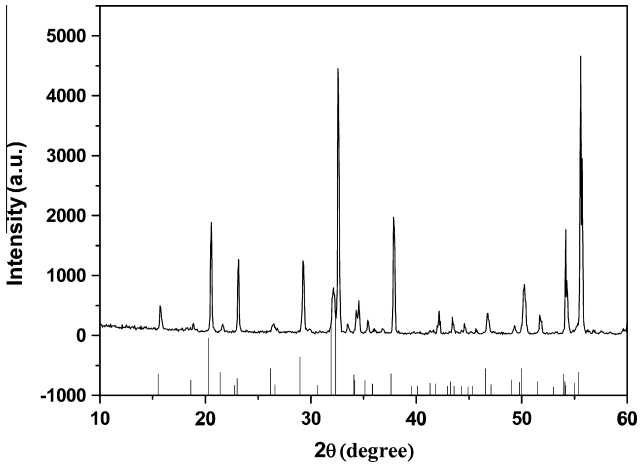

Fig. 2. XRD curve of the 0.5 wt.% Cr^{4+}:Ca_2GeO_4 crystal.

The lattice constants of the Cr^{4+}:Ca_2GeO_4 crystal can be obtained by the following calculation formula of the tetragonal system.

$$d = \frac{abc}{\sqrt{\ell^2a^2b^2 + h^2b^2c^2 + k^2a^2c^2}} \cdots \quad \cdots \quad (2)$$

d values can be obtained with Formula (1). We selected four different crystal plane (hkl) values, such as (111), (121), (200) and (002), and then we placed the corresponding d values into Formula (2) to produce four equations. The lattice constant has been obtained by solving equations with $a = 5.3209$ Å, $b = 6.6648$ Å, and $c = 11.2606$ Å. The results are very similar to those of the pure Ca_2GeO_4 phase. The lattice distortion caused by Cr^{4+} ions is quite small because the radii of the Cr^{4+} and Ge^{4+} are very similar.

3.2. Raman spectra

The Raman spectra of the Ca_2GeO_4 single crystal are shown in Fig. 3. The two strongest lines at 736 and 760 cm^{-1} in the Ca_2GeO_4 crystal are attributed to the $(GeO_4)^{4-}$ tetrahedral ν3 and ν1 stretching modes. The weak Raman peaks at 428 and 680 cm^{-1} are similar to those peaks that were reported in literature [20].

3.3. XPS analysis of the Cr^{4+}:Ca_2GeO_4 crystal

Fig. 4 shows the XPS survey spectra of the 0.5 wt.% Cr^{4+}:Ca_2GeO_4 crystal. Fig. 4 demonstrates that the Cr^{4+}:Ca_2GeO_4 crystal has Cr, Ca, Ge, O and C elements, where the C element is not an inherent component in the crystal. Information about the hydrogen element cannot be obtained from photoelectron spectroscopy, Thus, Cr^{4+}:Ca_2GeO_4 crystal may have an H-element.

The atomic concentrations of major elements and the peak banding energy of the elements in the crystal are shown in Table 1. The table dose not present the content of Cr element because the Cr^{4+} ion content in this crystal is less than the lowest measured value limits (0.1 mol%) used in the photoelectron spectroscopy, the content of the Cr element cannot be detected because of two main reasons. the sensitivity of the apparatus is low, the segregation coefficient of Cr element is small, which results in the low actual concentration of Cr^{4+} ions in this crystal.

In addition, the ratio of the main elements Ca:Ge:O is 1.98:1:4.15 in the crystal sample, but the ratio is 2:1:4 in Ca_2GeO_4 crystal. This difference is caused by impurities in the Ca, Ge, and O

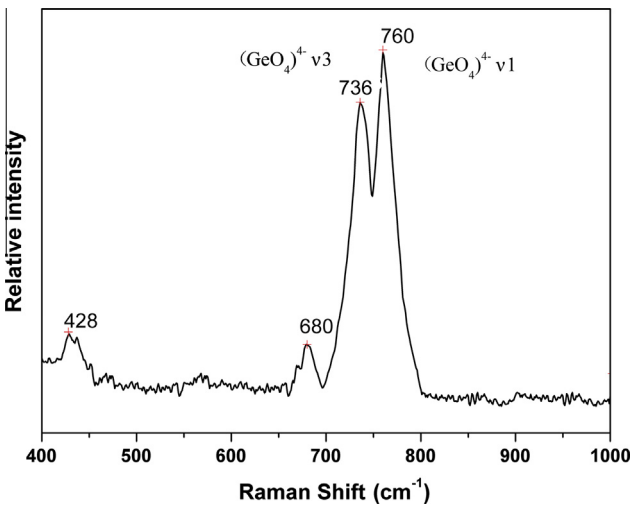

Fig. 3. Raman spectra of the Cr^{4+}:Ca_2GeO_4 polycrystallines.

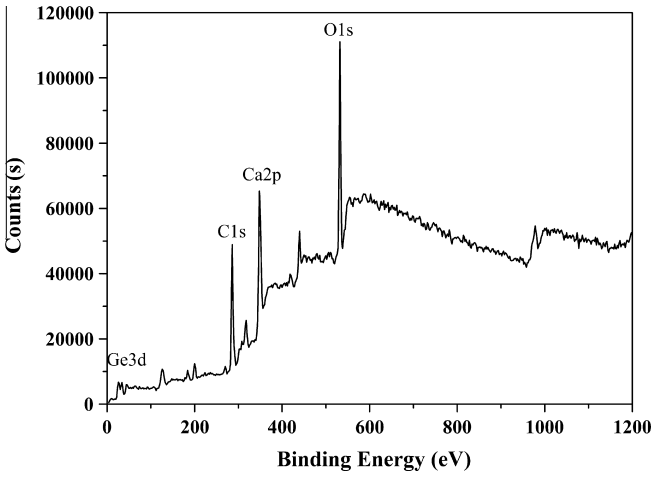

Fig. 4. XPS survey spectra of the Cr^{4+}:Ca_2GeO_4 crystal.

Table 1
Element concentration of Cr^{4+}:Ca_2GeO_4 crystal.

Elements	Peak BE (eV)	At.%
Ca2p	347	27.87
Ge3d	32	14.08
O1s	532	58.09

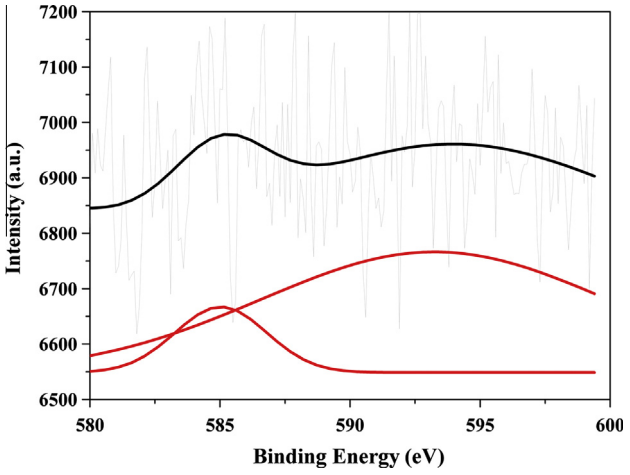

Fig. 5. Narrow scanning spectra of XPS for the Cr2p.

elements contained in the crystal sample and, perhaps, by a small amount of water on the crystal surface.

Fig. 5 shows the narrow scan spectra of XPS for Cr2p1/2. The XPS narrow scan spectra of the Cr2p peak is fitted by Gaussian equations. We obtained the Cr2p fitted peak at 584.5 eV [19], which corresponds to the Cr^{4+} ion. Therefore, the crystal contains only Cr^{4+} ions. This finding is consistent with the results of fluorescence spectroscopy analysis.

3.4. Absorption spectroscopy

Fig. 6(a) exhibits the absorption spectrum of the Cr^{4+}:Ca_2GeO_4 crystal in the region of 600–800 nm at room temperature. We assigned the strong absorption band at 647 nm, 686 nm and 731 nm to the transition of the Cr^{4+} ion from the $^3A_2$ ground state to the three different orbital components of the $^3T_1$ state (see Fig. 7), which are nearly completely polarized. According to the literature [18], three strong bands are assigned to the (6), (5) and (4) transitions, respectively. All other absorptions can be assigned to the vibrational sideband of these zero-phonon lines. The absorption spectrum of the Cr^{4+}:Ca_2GeO_4 crystal has evident red-shift compared with the absorption spectrum of Cr^{4+}:Mg_2SiO_4.

Fig. 6(b) shows the weak absorption spectrum of Cr^{4+}:Ca_2GeO_4 in the near infrared region at room temperature. Three relatively strong absorption peaks are located at 1002 nm, 1161 nm and 1200 nm. The absorption bands in the near-infrared region are assigned by the $^3A_2 \rightarrow {}^3T_2$ level transition of the Cr^{4+} ion. The three strong absorption peaks are assigned to the (3), (2) and (1) transitions. All other absorptions can be assigned to the vibrational sideband of these origins. The relatively low intensity of this absorption band can be attributed to the transition $^3A_2 \rightarrow {}^3T_2$, which is symmetry forbidden, although pronounced distortions of the local environment of the Cr^{4+} ion partially remove this prohibition.

3.5. Fluorescence spectrum

The emission spectra of 0.5 wt.% Cr^{4+}:Ca_2GeO_4 crystal, shown in Fig. 8 were measured for 824 nm and 808 nm excitation at room temperature and at low temperature. The fluorescence spectrum of Cr^{4+}:Ca_2GeO_4 crystal appears between 1000 and 1600 nm. This fluorescence results from the phonon-coupled $^3T_2 \rightarrow {}^3A_2$ transition of Cr^{4+} ions. The single band with a maximum peak at 1317 nm at room temperature is attributed to the Cr^{4+} ion, indicating that the crystal structure of the Ca_2GeO_4 allows only Cr^{4+} substitution. Cr^{4+} spectral signature does not exist. The single band with a maximum peak at low temperature is 1159 nm and 1207 nm.

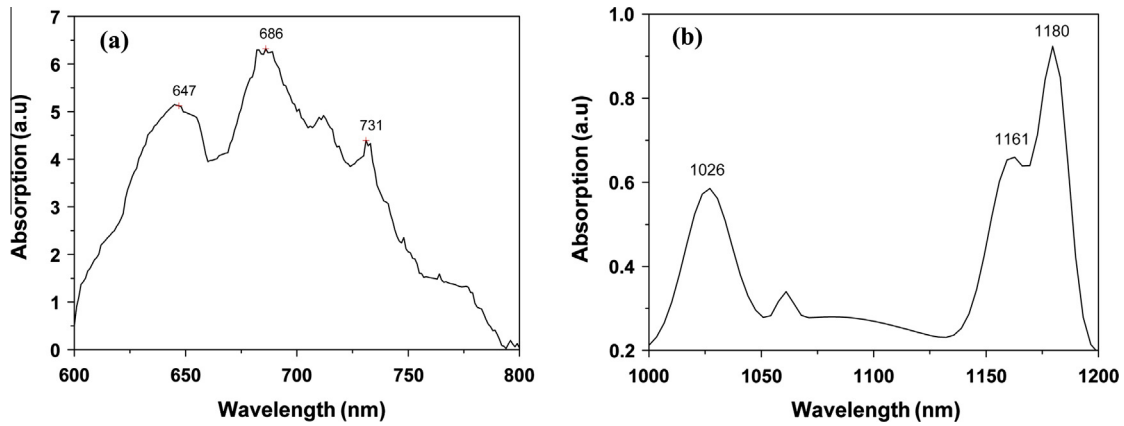

Fig. 6. Absorption spectrum of the Cr^{4+}:Ca_2GeO_4 crystal.

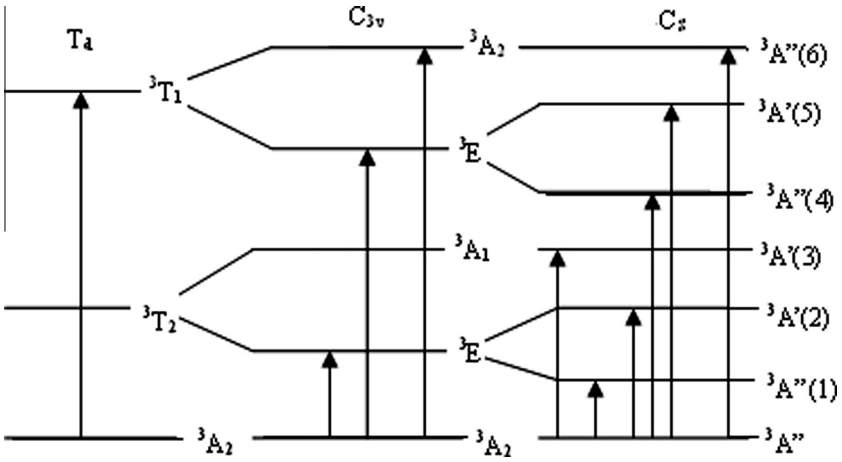

Fig. 7. Energy level of the Cr^{4+} ion.

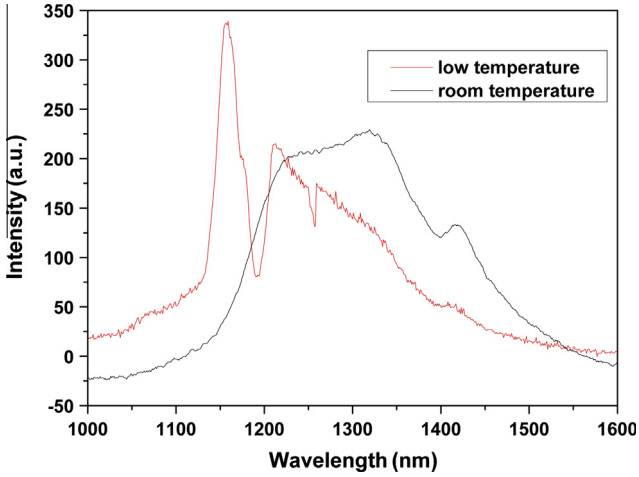

Fig. 8. Emission spectra of the 0.5 wt.% Cr^{4+}:Ca_2GeO_4 crystals at room and low temperatures.

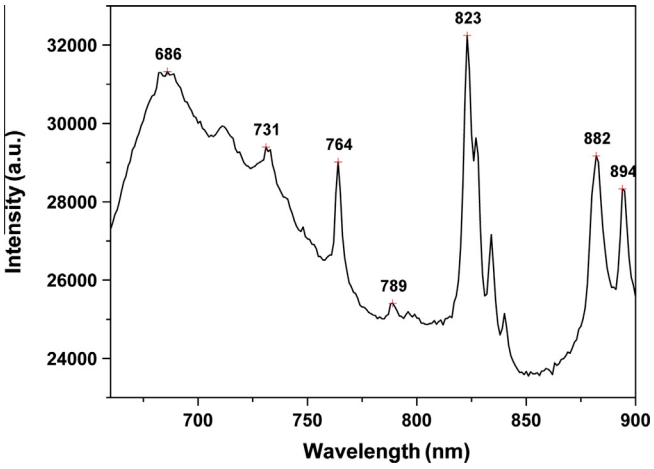

Fig. 10. Excitation spectra of the Cr^{4+}:Ca_2GeO_4 crystal.

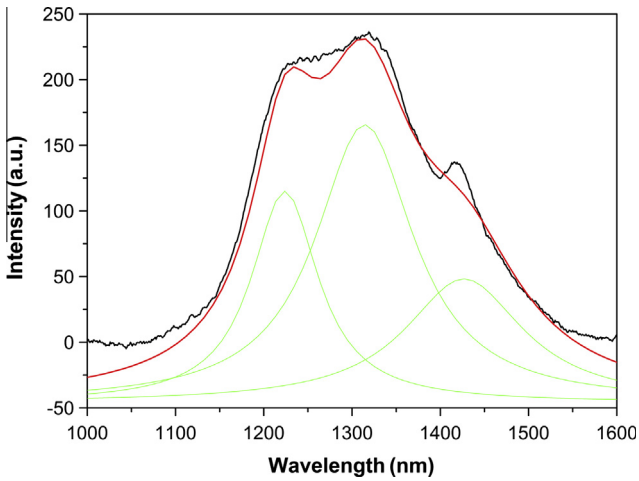

Fig. 9. Gaussian-fitted spectrum of the emission spectra of 0.5 wt.%.

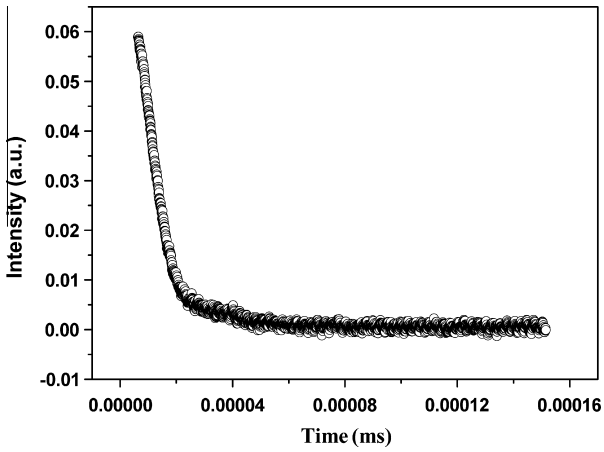

Fig. 11a. Fluorescence lifetime curve of the 0.1 wt.% Cr^{4+}:Ca_2GeO_4 single crystal.

Fig. 9 is illustrates the Gaussian-fitted spectrum of the emission spectra for 0.5 wt.% Cr^{4+}:Ca_2GeO_4 crystals at room temperature. We obtained three different fitting peaks located at 1223 nm, 1314 nm and 1426 nm. The different fitting peaks were assigned to the transition from the three different orbital components of $^3T_2$ excited state to the $^3A_2$ ground state.

The fluorescence emission cross section of the crystal is calculated with the following formula [17]:

$$\tau = \frac{1}{\sum A_{JJ'}} \tag{3}$$

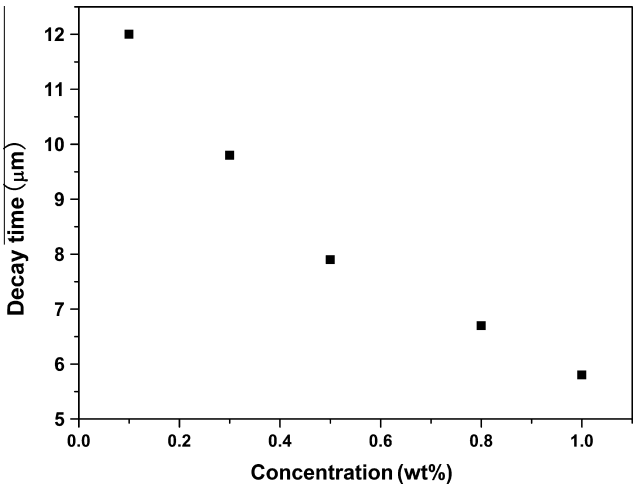

Fig. 11b. Dependence of the decay time of the Cr^{4+}:Ca_2GeO_4 on the Cr^{4+} concentration.

$$\sigma_{em}(\lambda) = \frac{\lambda^5 \eta I(\lambda)}{8\pi n^2 c\tau \int \lambda I(\lambda) d\lambda} \quad (4)$$

where c is the speed of light, n is the refractive index, τ is fluorescence lifetime, η is the radiative efficiency that can be estimated from the comparison between the theoretical radiative and the fluorescence lifetime, $I(\lambda)$ represents the experimental emission intensity as a function of the wavelength. According to Eq. (3), The FWHM of the fluorescence spectrum is 201.19 nm and the maximum emission cross-section is 4.61×10^{-19} cm^2.

Fig. 10 shows the excitation spectrum of the Cr^{4+}:Ca_2GeO_4 crystal at room temperature. Most of the bands observed in the absorption spectrum, such as 686 nm and 731 nm, are also observed in the excitation spectrum. The strongest stimulated peak is located at 823 nm.

The fluorescence lifetime of different doping concentrations of the Cr^{4+}:Ca_2GeO_4 single crystal are measured by Fluorolog—III fluorescence spectroscopy. The fluorescence lifetime curve is recorded by a TDS3012B oscilloscope. Fig. 11(a) is the fluorescence lifetime curve of a single 0.1 wt.% Cr^{4+}:Ca_2GeO_4 crystal, The decay curves for the luminescence of Cr^{4+} can be fitted by the single exponential function [21,22], $I = I_0 \exp(-t/\tau)$, where, τ is decay time, the decay time is 12 μs.

Fig. 11(b) shows the dependence of the luminescence lifetime of Cr^{4+} in Ca_2GeO_4 on the Cr^{4+} content. The fluorescence lifetime of a crystal decreases when the doping concentration increases, and they have linear relationship. At low Cr^{4+} concentrations (0–1.0 wt.%), the quantum efficiency of the Cr^{4+} centers, given by $\eta = \tau_{300K}/\tau_{77K}(Cr \rightarrow 0)$, is determined only by nonradiative relaxation. According to the literature [14], the fluorescence lifetime of the 0.1 wt.% Cr^{4+}:Ca_2GeO_4 crystal at the low temperature is 30 μs, so at 0.1 wt.% concentration, the quantum efficiency of the Cr^{4+} centers is 40%. At 1.0 wt.% concentration, the quantum efficiency of the Cr^{4+} drops to 25% because of the nonradiative relaxation and concentration quenching.

4. Conclusions

We have studied the growth, structure and spectrum properties of the Cr^{4+}:Ca_2GeO_4 crystal. The Raman spectra and XPS analyses demonstrated that a Cr^{4+}:Ca_2GeO_4 single crystal was successfully grown by the flux method. The XPS analysis and fluorescence spectroscopy indicate that only Cr^{4+} ion substitution occurs in the Cr-doped Ca_2GeO_4 single crystals although an oxygen atmosphere was used in the crystal growth process. This crystal represents a new tunable laser material.

Acknowledgements

This work was supported by the Science and Technology Department of Jilin Province (No. 201215177) and Changchun City Technology Bureau (No. 2014222). The authors also wish to thank Dr. Yue Xun and Dr. Liaohai Ge for carrying out the tensile tests.

References

[1] A. Agnesi, S. Dell'Acqua, P.G. Gobbi, Opt. Commun. 127 (1996) 273–276.
[2] A.R. Bijanzadeh, R. Khordad, Opt. Commun. 282 (2009) 2595–2603.
[3] John J. Zayhowski, J. Alloys Comp. 303–304 (2000) 393–400.
[4] K.V. Yumashev, I.A. Denisov, N.N. Posnov, N.V. Kuleshov, R. Moncorge, J. Alloys Comp. 341 (2002) 363–370.
[5] J. Zhao, S.Z. Zhao, K. Li, F.M. Kong, G. Zhang, Opt. Commun. 284 (2011) 1648–1651.
[6] Z. Sun, Q. Li, X. Chen, H. Lei, M.h. Jiang, Y.l. Hui, Opt. Laser Technol. 60 (2014) 56–60.
[7] Y. Kaliskya, O. Kaliskyb, M.R. Koktac, Opt. Mater. 30 (2008) 1775–1780.
[8] H. Chen, E. Wu, H.P. Zeng, Opt. Commun. 230 (2004) 175–180.
[9] Y.F. Chen, Y.C. Chen, S.W. Chen, Y.P. Lan, Opt. Commun. 234 (2004) 337–342.
[10] B. Henderson, H.G. Gallagher, T.P.J. Han, M.A. Scott, J. Phys.: Condens. Matter 12 (2000) 1927–1938.
[11] A. Sugimoto, Y. Nobe, K. Yamagishi, J. Cryst. Growth 140 (1994) 349–354.
[12] K. Watanabe, F. Taguchi, J. Cryst. Growth 131 (1993) 181–185.
[13] C.N. Tsai, K.Y. Huang, H.J. Tsai, J.C. Chen, Y.S. Lin, S.L. Huang, Y.S. Lin, J. Cryst. Growth 310 (2008) 2774–2779.
[14] M.Yu. Sharonov, S. Owen, A.B. Bykov, W.B. Wang, R.R. Alfano, Opt. Commun. 209 (2002) 209–216.
[15] H.M. Yang, J.X. Shi, M.L. Gong, H.B. Liang, Mater. Lett. 64 (2010) 1034–1036.
[16] C.X. Chen, S.P. Wu, Y.X. Fan, J. Alloys Comp. 578 (2013) 153–156.
[17] M.F. Hazenkampa, U. Oetlikera, H.U. Güdela, U. Kesperb, D. Reinenb, Chem. Phys. Lett. 233 (1995) 466–470.
[18] M.F. Hazenkamp, H.U. Güdel, M. Atanasov, U. Kesper, D. Reinen, Phys. Rev. B 53 (1996) 2367–2377.
[19] S. Fukaya, K. Adachi, M. Obara, H. Kumagaib, Opt. Commun. 187 (2001) 373–377.
[20] M. Yu Sharonov, A.B. Bykov, T. Myint, V. Petricevic, R.R. Alfano, Opt. Commun. 275 (2007) 123–128.
[21] G. Dominiak-Dzik, J. Alloys Comp. 391 (2005) 26–32.
[22] K. Maheshvaran, S. Arunkumar, V. Sudarsan, V. Natarajan, K. Marimuthu, J. Alloys Comp. 561 (2013) 142–150.